Integrative Biology, 2019, 1–11

doi: 10.1093/intbio/zyz028
Advance Access publication
Original Article

ORIGINAL ARTICLE

Substrate curvature induces fallopian tube epithelial cell invasion via cell–cell tension in a model of ovarian cortical inclusion cysts

Andrew J. Fleszar[1], Alyssa Walker[1], Pamela K. Kreeger[1,2,3,4,*,†], and Jacob Notbohm[1,2,5,*,†]

[1]Department of Biomedical Engineering, University of Wisconsin-Madison, Madison, WI 53706, USA, [2]University of Wisconsin Carbone Cancer Center, University of Wisconsin School of Medicine and Public Health, Madison, WI 53705, USA, [3]Department of Obstetrics and Gynecology, University of Wisconsin School of Medicine and Public Health, Madison, WI 53705, USA, [4]Department of Cell and Regenerative Biology, University of Wisconsin School of Medicine and Public Health, Madison, WI 53705, USA, and [5]Department of Engineering Physics, University of Wisconsin-Madison, Madison, WI 53706, USA

*Corresponding authors. E-mail: kreeger@wisc.edu; jknotbohm@wisc.edu
†Author contributed equally.

Abstract

Throughout the body, epithelial tissues contain curved features (e.g. cysts, ducts and crypts) that influence cell behaviors. These structures have varied curvature, with flat structures having zero curvature and structures such as crypts having large curvature. In the ovary, cortical inclusion cysts (CICs) of varying curvatures are found, and fallopian tube epithelial (FTE) cells have been found trapped within these cysts. FTE are the precursor for ovarian cancer, and the CIC niche has been proposed to play a role in ovarian cancer progression. We hypothesized that variations in ovarian CIC curvature that occur during cyst resolution impact the ability of trapped FTE cells to invade into the surrounding stroma. Using a lumen model in collagen gels, we determined that increased curvature resulted in more invasions of mouse FTE cells. To isolate curvature as a system parameter, we developed a novel technique to pattern concave curvatures into collagen gels. When FTE cells were seeded to confluency on curved substrates, increases in curvature increased the number of invading FTE cells and the invasion distance. FTE invasion into collagen substrates with higher curvature depended on matrix metalloproteinases (MMPs), but expression of collagen I degrading *Mmps* was not different on curved and flat regions. A finite-element model predicted that contractility and cell–cell connections were essential for increased invasion on substrates with higher curvature, while cell–substrate interactions had minimal effect. Experiments supported these predictions, with invasion decreased by blebbistatin, ethylene glycol-bis(β-aminoethyl ether)-N,N,N',N'-tetraacetic acid (EGTA) or N-cadherin-blocking antibody, but with no effect from a focal adhesion kinase inhibitor. Finally, experimental evidence supports that cell invasion on curved substrates occurs in two phases—a cell–cell-dependent initiation phase where individual cells break away from the monolayer and an MMP-dependent phase as cells migrate further into the collagen matrix.

Keywords: cell-cell adhesion; curvature; ovarian cancer; fallopian tube eptihelial cells; cellular mechanics

Received July 2, 2019; **revised** September 3, 2019; **editorial decision** September 4, 2019; **accepted** September 4, 2019

INSIGHT, INNOVATION AND INTEGRATION

Curved epithelial tissues occur throughout the body, yet the impact of substrate curvature on epithelial cell behavior remains unclear. In this study, we developed 3D printed molds to pattern collagen I hydrogels with a flat surface or concave curves of different curvatures. We found that fallopian tube epithelial (FTE) cells did not invade on flat gels but underwent spontaneous invasion on curved collagen substrates, and invasion increased as curvature increased. By using a finite-element model to inform experimental conditions, we discovered that cell–cell tension transmitted by N-cadherin induced the invasion of FTE cells into collagen I gels within the curve, while MMP activity regulated the distance of invasion into the matrix.

INTRODUCTION

In the human body, cells are organized into structures that give rise to unique tissues. One of the most widespread tissues is the epithelium, which is comprised of epithelial cell monolayers that line the surfaces of organs. These epithelial cell monolayers commonly cover extracellular matrix (ECM) substrates with curved topography, such as ducts in the breast, pancreas, and kidney and crypts in the small intestine [1–4]. Over the past 20 years, the field of mechanotransduction has revealed that the substrate beneath a cell can impact behaviors including proliferation, invasion, migration and apoptosis; however, most studies have focused on how changes in substrate stiffness and ECM composition impact these behaviors in the context of flat surfaces, which by definition have zero curvature [5–9]. Meanwhile, the impact of substrate curvature on epithelial cell behavior has been less rigorously explored.

Initial experiments investigating the impact of substrate curvature on epithelial cell behavior cultured rat liver (IAR-2) and dog kidney (MDCK) epithelial cells as individual cells on cylindrical glass rods and observed that a curved substrate causes circumferential alignment of actin stress fibers [10, 11]. A more recent study demonstrated that stress fiber alignment in fibroblasts depends on position within the cell, with basal stress fibers aligning in the circumferential direction and apical stress fibers aligning along the cylinder's axis [12]. Cell response to substrate curvature also depends on whether the cell is isolated or within a confluent group. On convex substrates, confluent layers of cells show stronger alignment than single cells in the direction perpendicular to the curve [12]. Confluent layers of cells respond to curvature on concave substrates as well, with the magnitude of curvature affecting the amount of cell alignment [13]. Forces between cells on concave substrates are pronounced, as demonstrated by a study that seeded confluent layers of cells on concave substrates and observed them to detach from the concave region, forming a one-cell-thick bridge [14].

Many human ovaries contain cortical inclusion cysts (CICs), which are spherical or oval epithelial-lined cysts found within the cortex of the ovary. CICs are thought to arise from ovulation wounds and age-related invagination of the ovarian surface [15–17]. While CICs are most commonly lined with ovarian surface epithelial cells, fallopian tube epithelial (FTE) cells have been found trapped within them, as either a mixed population of ovarian surface epithelium or predominantly FTE [18]. As FTE are believed to be the precursor cell for many high-grade serous ovarian cancers [19], the niche environment of these cysts has been hypothesized to aid in the progression of ovarian cancer [18]. Furthermore, CICs are an interesting model system to study the effects of curvature because these cysts shrink as they resolve, and cells in CICs are, therefore, subjected to increasing curvature over time [20].

We have previously developed a microfluidic lumen model of CICs and demonstrated that FTE cells invaded into the collagen matrix surrounding the lumen [21]. We hypothesized that the increase in curvature that occurs during CIC resolution provides a mechanism for FTE cells to transition to an invasive phenotype. To test this hypothesis, we developed a novel system of 3D printed molds to pattern varied curvatures into collagen I substrates and generated a finite-element (FE) model to examine how cell–cell and cell–substrate interactions impact the behavior of cells on curved substrates. Lastly, we used a series of drug-inhibition studies to test the FE models predictions *in vitro*.

METHODS

Cell lines and reagents

Unless otherwise stated, all reagents were purchased from ThermoFisher (Waltham, MA). Mouse FTE cells expressing a loss of function, dominant negative mutated $p53^{R273H}$ protein were obtained from Dr. Joanna Burdette at the University of Illinois at Chicago [22]. We selected to use FTE cells expressing mutated p53 as FTE cells are the cell of origin for ovarian cancer and the initiating genomic change for most tumors is mutation in *TP53* [23]. Histological and genomic studies have demonstrated that this change occurs prior to metastasis to the ovary [24–26]. Therefore, to analyze cancer progression in the ovary, the cells must be of fallopian origin and express nonfunctional p53. Cells were maintained at 37°C in 5% CO_2 in minimal essential medium (MEM) alpha modification supplemented with 10% heat-inactivated fetal bovine serum (FBS), 2 mM of L-glutamine (Sigma-Aldrich; St. Louis, MO), 2 ng/ml of epidermal growth factor, 5 µg/m of insulin (Roche; Basel, Switzerland), 5 µg/ml of transferrin (Roche), 5 ng/ml of sodium selenite (Roche), 1.1 µg/ml of gentamicin (Corning; Corning, NY) and 0.055% penicillin/streptomycin.

Microfluidic lumen fabrication

Microfluidic lumens were made using the LumeNEXT platform (Supplementary Fig. 1A, [21, 27]. Briefly, soft lithography was used to generate negative molds of the multilayer lumen device, and polydimethylsiloxane (PDMS; Dow Corning; Salzburg, MI) prepared at a 1:10 ratio of curing agent to elastomer base was used to fabricate the top and bottom layers of the chamber. Linear PDMS rods with 400 and 205 µm radii were created by filling 22G and 27G hypodermic needles with PDMS and removing the

PDMS from the needles after curing. These circular lumen rods were inserted into the chamber, and the devices were bonded to a glass surface using oxygen-plasma treatment (Thierry Corp.; Royal Oak, MI).

Collagen substrate formation around lumens

Microfluidic lumen devices were sterilized by exposure to UV light for 20 min, pretreated with 4% poly(ethylenimine) (Sigma) diluted in sterile deionized water for 10 min at room temperature followed by 0.2% glutaraldehyde (Sigma) diluted in sterile deionized water for 30 min at room temperature and washed three times with sterile deionized water. Collagen gel preparation was carried out on ice to inhibit collagen polymerization. Nine parts of rat tail collagen type I was mixed with one part of neutralization solution to achieve a final concentration of 3.6 mg/ml (Advanced Biomatrix; Carlsbad, CA); this concentration was selected based on our previous characterization of the collagen I levels surrounding CICs in human ovaries [21]. The mixture was incubated on ice for 20 min before use. The collagen gel mixture was loaded into each lumen device, and the devices were surrounded by a ring of 200 µl of phosphate buffered saline (PBS) to provide humidity. The devices were incubated at room temperature for 10 min followed by overnight incubation at 37°C. On the following day, 5 µl of PBS was added to the small port of each lumen and the PDMS rod was pulled out of the polymerized collagen from the larger port, resulting in a lumen structure filled with PBS inside a collagen I gel.

Cell seeding and culture in lumens

FTE cells were stained with 2-µM CellTracker™ Green following manufacturer's directions, dissociated using trypsin–EDTA, passed through a 40-µm cell strainer (Corning), and suspended in media at 100,000 cells/µl. The lumens were washed once with PBS, 4 µl of cell suspension was added to each lumen through the small port, and the PBS ring surrounding the device was replenished. The lumens were rotated at 3 rpm for 2 h at 37°C, washed once with 5 µl of media to remove unattached cells, and incubated with 5 µl of media per lumen. The devices were rotated at 3 rpm throughout the experiment, and the media in the lumens and the PBS ring around the device were changed every 12 h. Prior studies [21] have demonstrated that ovarian surface epithelium, another ovarian cell found in CICs, did not invade from lumens. As CICs can be lined with FTE, ovarian surface epithelium or a mixed population, we briefly examined co-cultures of FTE and mouse ovarian surface epithelial cells and observed that only FTE cells invaded (Supplementary Fig. 1B); therefore, only FTE cells were used in all other experiments presented here.

Curvature negative molds

Negative molds for collagen gels were designed using Solidworks (Dassault Systèmes; Waltham, MA, USA) to either have a flat or curved surface. For the curved surface, the depth was kept constant at 400 µm and the curvature was altered by controlling the radius, which is mathematically equal to the inverse of curvature. Radii were either 3200 µm (low curvature) or 400 µm (high curvature, equivalent to a half circle). Molds were 3D printed on a Form 2 printer (Formlabs; Somerville, MA) using Durable Form 2 Print resin (Formlabs). Molds were cleaned with 70% ethanol before each use.

Curved collagen substrate formation

Falcon 8-well culture slides (Corning; Corning, NY) were exposed to an oxygen-plasma treatment to make the surface of the slides hydrophilic. The culture slides were sterilized by exposure to UV light for 20 min, pretreated with 4% poly(ethyleneimine) diluted in sterile deionized water for 10 min at room temperature followed by 0.2% glutaraldehyde diluted in sterile deionized water for 30 min at room temperature and washed three times with sterile deionized water. After washing, a 3D printed negative mold was placed into each well of the eight-well chamber slide.

Collagen gel solution was prepared as above, and 150 µl was loaded into each well of the eight-well culture slide in the gap between the mold and the bottom of the slide. Culture slides were placed in a 14-cm petri dish, and two Kimwipes were soaked in PBS and added into the petri dish to provide humidity. The devices were incubated at room temperature for 10 min followed by overnight incubation at 37°C. On the following day, 400 µl of PBS was added to each well of the chamber slides and the molds were removed, resulting in collagen I substrates with either a flat surface or a concave curve (Supplementary Fig. 1C).

Cell seeding on curvature devices

FTE cells were dissociated using trypsin–EDTA, passed through a 40-µm cell strainer, and suspended in media at 1.3 million cells/ml. The collagen gels were washed once with PBS, 400 µl of cell suspension was added to each curvature device, and the device was incubated on a flat surface for 10 min, followed by 10 min incubation at a 30° angle on each side to better allow cells to attach to the sides of the curve. The flat and angled incubations were repeated one additional time, and the devices were then incubated on a flat surface for 5 h to allow cell–cell junctions to form. The media was changed 6 h after seeding and every 24 h throughout culture.

Interventions in cell invasion experiments

Specific myosin II inhibitor blebbistatin (20 µM, Sigma) [28], focal adhesion kinase (FAK) inhibitor 14 (10 µM, Sigma) [29], EGTA (10 mM, Sigma) [30, 31] and matrix metalloproteinase (MMP) inhibitors GM6001 (20 µm, EMD Millipore; Burlington, MA) [32] and batimastat (20 µM, Tocris Biosciences; Bristol, UK) [33] were diluted in media. Unless otherwise specified, drugs were added to cultures during the initial media change (6 h after seeding).

To determine the role of N-cadherin in invasion, cells were incubated with 200 µg/ml of anti-N-cadherin-blocking antibody (Clone GC-4, Sigma) [34] or monoclonal mouse IgG1 isotype control for 1 h at 37°C. To prevent aggregation, cells were rotated at three rpm throughout the incubation. Cells were then seeded in the devices as described above and antibodies were replaced every 24 h.

RT-PCR for *Mmps*

Cells were cultured on curved collagen gels for 48 h; gels were then cut into three sections—one curved region and two plateau regions—using a razor blade (Supplementary Fig. 1C). Curved and plateau regions were separated and then pooled across six collagen gels. The resulting curved or plateau samples were placed into 350 µl of buffer RLT (Qiagen; Valencia, CA), passed through a 22G needle five times, and then passed through a 27G needle five times. RNA was collected and isolated using the Micro-

RNeasy Extraction kit (Qiagen), and cDNA was synthesized using the Qiagen FirstStrand Kit according to manufacturer's instructions. qRT-PCR was performed using mouse primers for *Mmp-1a, Mmp-2, Mmp-8, Mmp-9, Mmp-13, Mmp-14* and *Gapdh* (all Qiagen) with SsoAdvanced Universal SYBR Green Supermix (Bio-Rad; Hercules, CA). PCR was run on a CFX real-time PCR machine (Bio-Rad) for a total of 40 cycles, and three samples were run in duplicate for each condition. Data are expressed as fold change, with ±2-fold set as the threshold for significance.

Analysis of cell invasion

A Leica TCS SP8 confocal microscope (Leica; Wetzlar, Germany) was used to image cells in lumens and on curved substrates. For lumens, the number of invading cells was measured from a confocal slice taken at the midpoint of each lumen [21]. For cells on curved substrates, confocal z-stacks capturing the curved region of the gel and invading cells were resliced using FIJI to obtain side view of z-stacks of the curved substrate (Supplementary Fig. 2). Each z-stack was then projected using average intensity into a single image. From this side view, a region containing cells seeded on top of the substrate was manually outlined and deleted from the side view of z-stack. The remaining z-stack contained the side view of cells that invaded into the substrate in the region below the curve, and the distance of invasion for each cell was measured from this stack. This z-stack was then resliced and projected in FIJI to obtain a single top-down image of only the invading cells. This image was thresholded using the default settings in FIJI, and the number of invading cells was measured by analyzing particles larger than 40 μm^2.

FE model

An FE model was developed in Abaqus 6.12 (Dassault Systèmes) to compute the forces of cell contraction on the curved substrates. As the geometry of the experiments does not vary out of the plane of the curve, a two-dimensional model was used. Linear, 4-node, plane stress elements were used to simulate both the cells and substrate. The substrate geometry matched the experiments with a total height of 1 mm and concave regions having radii of curvature of 3200 μm (low curvature) or 400 μm (high curvature). Each cell consisted of twelve elements and was connected to its neighbors and to the substrate with linear springs at each node [35, 36]. The Young's modulus of the substrate was taken to be 1.7 kPa, as specified by the supplier of collagen used in the experiments (Advanced Biomatrix). Though the Young's modulus of the cell layer was unknown, previous studies have suggested moduli of epithelial cells ranging from 0.1 to 10 kPa, with a typical value of 1 kPa [37–40]. We therefore performed simulations for cell layers having Young's moduli if 0.1, 1 and 10 kPa and observed trends in the data to be the same in all cases. Poisson's ratio similarly had minimal effect on the results, and a value of 0.3 was used for both the cells and the substrate. Cell contraction was simulated by imposing a thermal strain to the cell elements. Note that the product of Young's modulus and thermal strain sets the magnitude of stress in the results; increasing (decreasing) either modulus or thermal strain causes a proportional increase (decrease) in the computed stress. A symmetric boundary condition was used to simulate half of the geometry; the nodes at the bottom of the substrate were assigned a fixed boundary condition. The normal stress between cells and substrate was computed by outputting the normal force in the springs between cells and substrate and dividing by area over which each spring acted, which was equal to the product of the distance between the springs and the unit thickness. The stiffness of the springs was chosen by first identifying the upper bound k_{max}, which is related to the Young's modulus of the cell layer E by the equation $k_{max} = EL/s$ [36], where s is the spacing between springs and the length L is ≈1 due to the fact that the modeled cells are nearly square with unit thickness. This estimate gives $k_{max} = 20, 200$ and 2000 N/m for cell layers having moduli of 0.1, 1 and 10 kPa, respectively. The values of k_{max} used were validated by sensitivity studies, which indicated that values of spring stiffness greater than k_{max} had no effect on the results. A similar sensitivity study demonstrated that values of spring stiffness less than $0.01 \times k_{max}$ had no effect on the results. To span the full range of possible stiffness, three values of spring stiffness were chosen with magnitudes of $0.01 \times k_{max}$ (referred to as 'compliant'), $0.1 \times k_{max}$ (referred to as 'intermediate') and k_{max} (referred to as 'rigid'). For a cell layer having a modulus of 1 kPa, the corresponding values of stiffness are 2, 20 and 200 N/m, respectively.

Statistics

All data are presented as mean ± standard deviation. The number of invading cells includes the results of multiple independent experiments, with the total number of lumens/gels per condition noted in each legend. Invasion distances are provided from one representative experiment due to day-to-day variation in baseline invasion, and the number of cells per condition is provided in each legend. All experiments were performed at least twice (results for all repeats are provided in Supplementary Table 1). Statistical calculations were performed in GraphPad Prism software (La Jolla, CA).

RESULTS AND DISCUSSION

FTE cell invasion increases with increased curvature in lumens

We have previously shown that FTE cells invade into collagen when cultured in a microfluidic lumen model that mimics CICs, but not when cultured on flat collagen substrates [21]. In these prior studies, lumens were made with high curvature (205 μm radius; recall that curvature is the mathematical inverse of radius); however, histological measurements of human ovaries demonstrated that CICs encompass a broad range of curvatures. When CICs were approximated as a circle and measured, the 25th percentile radius was 112 μm, the median radius was 254 μm, and the 75th percentile radius was 605 μm [21]. CICs are hypothesized to form from ovulation wounds or invaginations of the ovarian surface, and the randomness of these processes likely results in variation in the initial curvature of CICs across patients, between CICs in the same ovary, and within a single CIC as they are not perfectly circular [41, 42]. An additional source of variation in CIC curvature occurs over time, because the CIC shrinks in size as it resolves [20]. Therefore, we investigated the impact of CIC curvature on cell invasion by seeding FTE cells in microfluidic lumens with low curvature (400 μm radius) and high curvature (205 μm radius) (Fig. 1A), which are representative of smaller ovarian CICs (Fig. 1B). The number of invading cells was measured from a confocal z-slice taken at the midplane of each lumen (Fig. 1C), and the results showed that increasing the curvature significantly increased the number of FTE cells that invaded into the surrounding collagen I matrix (Fig. 1D). As FTE cells, the precursors for high-grade serous ovarian cancer, have

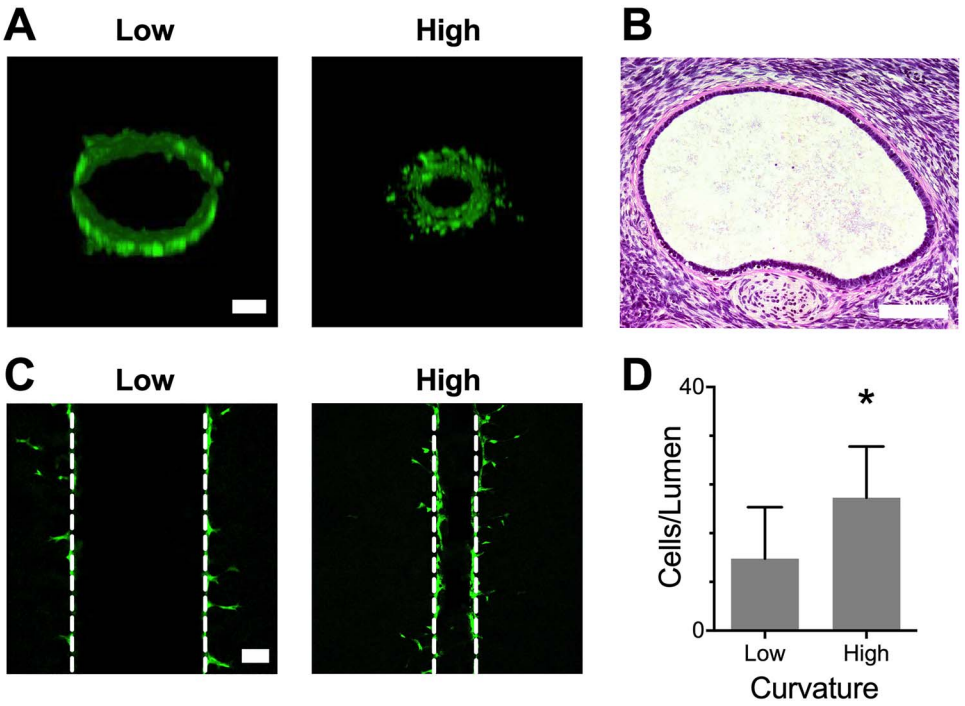

Figure 1. Increasing curvature increased FTE cell invasion in a microfluidic lumen model of ovarian CICs. A) Z-stack cross-section reconstruction of CellTracker^{TM} Green-labeled FTE cells seeded in lumens with low- (400 μm radius) and high-curvature (205 μm radius) lumens. Scale bar = 100 μm. B) H&E stain of a representative ovarian CIC. Scale bar = 200 μm. C) Confocal slices taken at the midplane of lumens with low- and high curvature from which the number of invading cells were measured. Scale bar = 100 μm. D) Increasing curvature in microfluidic lumens increased the number of invading FTE cells per lumen, $n = 25$ lumens for low curvature and 26 lumens for high curvature. * indicates $P < 0.0001$ using a two-sided t-test.

been observed within ovarian CICs, this observation suggests that the increase of curvature associated with CIC resolution may allow FTE cells trapped within a CIC an opportunity to escape [20].

FTE cell invasion increases with increasing curvature on engineered substrates

Changing the curvature of the microfluidic lumens also changed the ratio of surface area to volume within the lumens. It has been hypothesized that the large surface area to volume ratio and enclosure of ovarian CICs leads to the accumulation of cytokines and growth hormones and initiates cell signaling [16, 43]. Increased levels of IL-1 and IL-6, which are secreted by cells on the surface of the ovary [44], enhance the proliferation of ovarian tumors [17], and the accumulation of other cytokines and hormones may lead to dysplasia [45]. In contrast to cell signaling that can be amplified when the ligand is concentrated [43], the impact of variations in curvature on cell behavior has not been explored. In order to isolate curvature as a system variable without impacting concentration of factors in the media, we designed a novel system to pattern curved substrates in collagen gels (Supplementary Fig. 1C). Using this system, negative molds with either a flat surface, convex high curvature (comparable to the low curvature examined in lumens) or convex low curvature (comparable to larger CICs) were fabricated using a 3D printer. By polymerizing collagen I between the molds and the bottom of an eight-well chamber slide, substrates with concave curves between two flat plateau regions were formed. FTE cells were seeded to confluency on these curved substrates and allowed to form cell–cell interactions. A preliminary study was carried out to investigate the effects of curvature on cell seeding. Substrates having larger curvatures than that used in our study were not able to be seeded uniformly due to challenges in seeding cells as we could not use the rotation method employed with lumens. Imaging and quantification of cell nuclei indicated that all substrates used in our study (flat, low curvature and high curvature) were seeded uniformly (Supplementary Fig. 3A) and that the cell density was the same across conditions (Supplementary Fig. 3B), ensuring that changes in cell behavior observed in curved regions were not an artifact of cells settling to the bottom of the curve during seeding.

After FTE cells were seeded to confluency on substrates with different curvatures, the cells invaded into the collagen I substrates, similar to the invasion observed in lumens (Fig. 2A). As shown in the representative cross-sectional images of cells on flat, low curvature and high curvature substrates, cell invasion did not occur on flat gels or in the plateau regions on each side of the curve. As curvature increased, invasion increased, with significantly more cells invading into high-curvature substrates compared to both the flat and low-curvature substrates (Fig. 2B). This finding was consistent with our observations in the lumen model. Thus, the monolayer of cells responded to curvature that was at least an order of magnitude greater than the curvature of a single cell, which highlights the importance of studying the cells as a collective. In addition, the distance that invading cells moved into the collagen was significantly greater from the high-curvature compared to the other conditions (Fig. 2C). Our prior results demonstrated that global collagen concentration impacts cell invasion from a lumen [21]. To verify that changing curvature in our assay had no effect on collagen concentration, we measured collagen pore size on flat and curved substrates and observed no difference (Supplementary Fig. 4A). We next questioned whether a relationship between curvature and col-

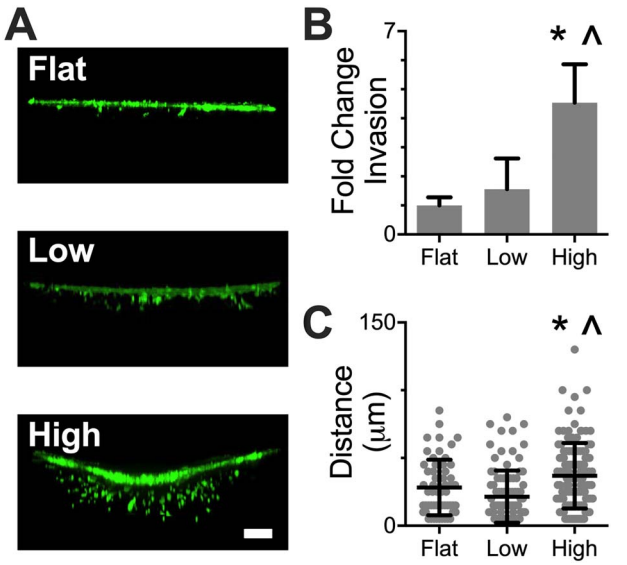

Figure 2. Increasing curvature increased the number and distance of FTE cell invasion. A) Z-stack cross-section reconstruction of CellTracker Green stained FTE cells seeded on collagen I gels with a flat surface, low curvature or high curvature. Scale bar = 100 μm. B) Increasing curvature increased the number of cells that invade. $n = 8$ gels for flat and low curvature; 9 gels for high curvature. C) Increased curvature increased invasion distance of FTE cells. $n = 56$ cells for flat, 94 cells for low curvature, and 127 cells for high curvature. * indicates $P < 0.05$ relative to flat, and ^ indicates $P < 0.05$ relative to low curvature by Tukey.

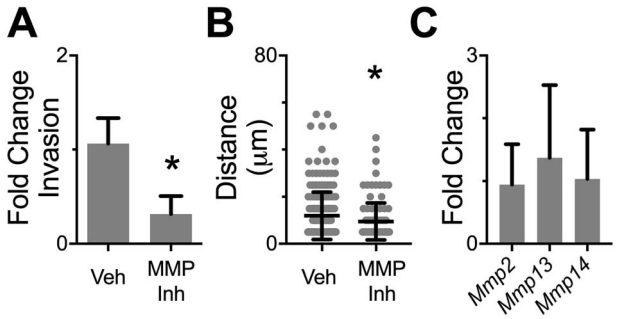

Figure 3. MMPs were required for invasion but were not upregulated on curved substrates. A) The number of invading cells on high-curvature substrates was reduced with treatment with GM6001 and batimastat (MMP Inh). $n = 17$ gels for vehicle, 16 gels for MMP inhibition. B) The average invasion distance was decreased with GM6001 and batimastat. $n = 222$ cells for vehicle; 110 cells for MMP inhibition. C) Fold change in expression for *Mmp*-2, *Mmp*-13 and *Mmp*-14 was less than two between cells on curved regions and plateau regions of collagen I hydrogels. Other *Mmps* that were tested were not detected over 40 PCR cycles. $n = 3$. * indicates $P < 0.05$ using a two-sided t-test.

lagen density exists *in vivo*. Using data acquired in our prior work [21], we compared density of ECM surrounding human ovarian CICs to curvature, and found no relationship between curvature and concentrations of either collagen I or collagen III (Supplementary Fig. 4B,C). Taken together, these data indicate that low curvature, as would be expected in a larger CIC would have minimal impact on FTE cell invasion. However, as the CIC resolves, it decreases in size, causing an increase in curvature that may transition FTE cells to an invasive phenotype. Our prior results demonstrated that FTE invasion from the CIC is also impacted by changes in the soluble factors present and the ECM density/composition of the surrounding stroma [21]. Combined, these results help to demonstrate why despite the broad presence of CICs in the ovary, ovarian cancer remains relatively rare [46] as variations in the microenvironment impact the ability of FTE to progress toward a cancerous phenotype.

MMPs are necessary for invasion but expression is not altered by curvature

Cell invasion into the extracellular matrix commonly requires matrix remodeling by MMPs, a family of proteases that degrade ECM with MMP–ECM specificity [47]. We hypothesized that MMPs were necessary for invasion of FTE cells, and that the changes in invasion associated with substrate curvature may result from curvature-induced changes in expression of collagen I-degrading MMPs. To test this hypothesis, cultures were treated with vehicle or a combination of two broad-spectrum MMP inhibitors (batimastat and GM6001), which inhibit all MMPs that degrade collagen I. We examined the impact of this inhibition in the high-curvature condition, as this culture setup contains both the highest invasion (within the curve) and the lowest invasion (from the flat regions surrounding the curve). MMP inhibition significantly reduced the number of invading cells in the curve (Fig. 3A); as in Fig. 2, cells did not invade on the plateau region in either condition (data not shown). Inhibiting MMPs also significantly decreased the distance that cells invaded (Fig. 3B). As the media from cultures contained secreted factors from both cells on the curve and cells on the plateau, we were unable to determine if curvature impacted the protein level or activity of MMPs. Instead, we examined if gene expression for *Mmps* was different between curved and flat regions by cutting the culture device into three sections (i.e. the two plateaus on the sides and the curved region in the center, Supplementary Fig. 1C). The relative levels of collagen I degrading collagenases (*Mmp-1a*, *Mmp-8* and *Mmp-13*) and gelatinases (*Mmp-2*, *Mmp-9* and *Mmp-14*) were then compared between curved and plateau regions by qRT-PCR. *Mmp-1a*, *Mmp-8* and *Mmp-13* were not detected after 40 PCR cycles, suggesting they were expressed at very minimal levels by FTE cells on either curved or flat substrates. Additionally, the levels of *Mmp-2*, *Mmp-13* and *Mmp-14* did not significantly vary between curved and plateau regions (Fig. 3C). Taken together, these data indicate that MMPs are necessary for curvature-based invasion, but curvature does not increase invasion into a collagen I substrate through a mechanism involving a transcriptional program to upregulate *Mmp* expression.

FE model of cells on curved substrates

The lack of *Mmp* upregulation on curved collagen I substrates suggested that while MMPs facilitate migration after cells begin to invade, matrix remodeling is not involved in the initiation of invasion. To identify the mechanism responsible for initiation, we began with the observation that the curvatures affecting invasion would be sensed by a single cell as being essentially flat. Therefore, the curvature is sensed at the scale of the monolayer rather than that of a single cell. By contrast, invasion occurs by individual cells, indicating that some mechanism must transmit a multicellular cue, curvature, to the scale of an individual cell. A potential mechanism is mechanical force, which would be altered globally by curvature and sensed locally by a single cell. Force has also been related to cell invasion by experiments that observed cell spreading along directions of tensile matrix stretching [48]. We therefore hypothesized that curvature altered the normal stress applied by cells to the substrate in the direction of invasion.

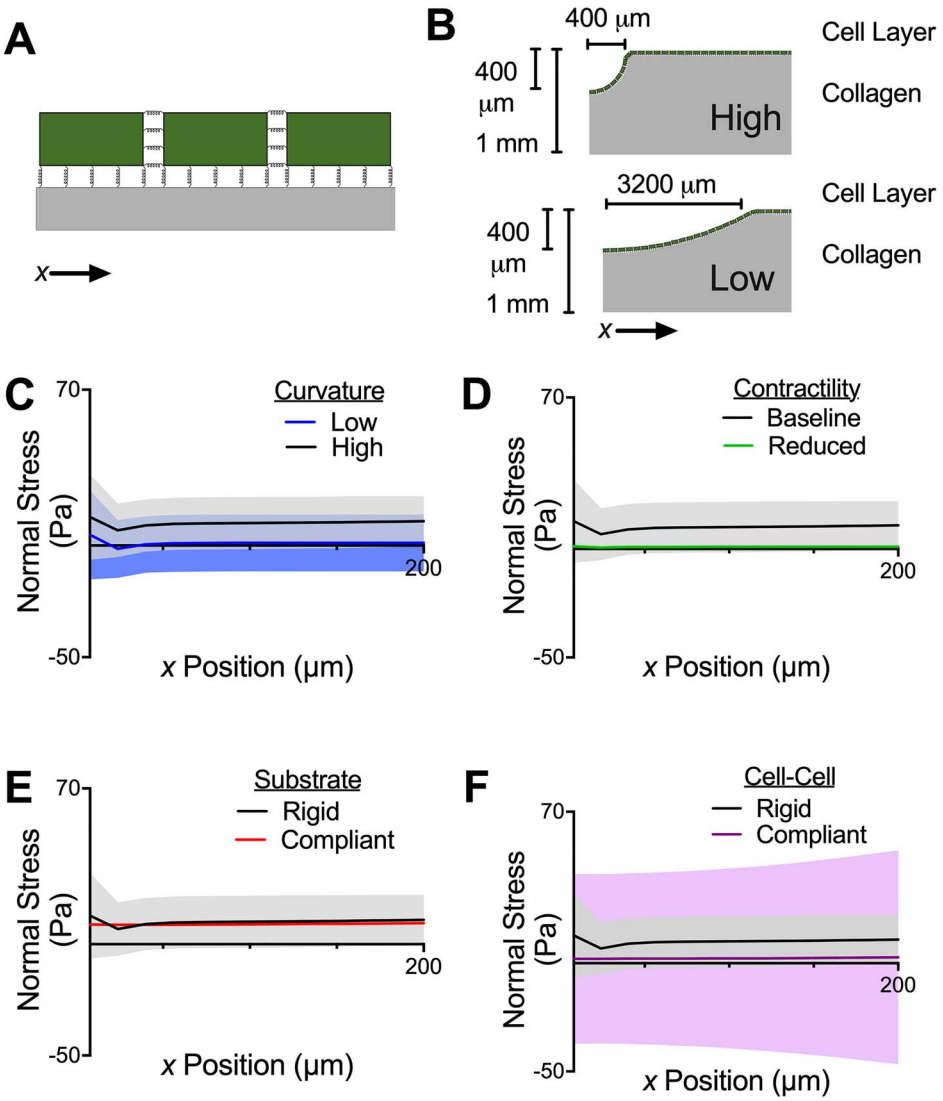

Figure 4. FE model of cells on curved substrates. A) Schematic showing the basic structure of the FE model. Cells (green) are connected to each other and the substrate (gray) via springs. B) Schematic showing dimensions of the FE model on substrates with low and high curvatures. C) Increasing curvature increases the normal stress between cells and the substrate within 200 μm of the center of the curve. Solid lines show the mean of the normal stress applied by each cell; shaded areas show the standard deviation. D) Reducing contractility within the cell monolayer by a factor of 10 decreases the average normal stress per cell and the variation between springs within each cell. E) Adjusting springs connecting cells to the substrate from rigid to compliant has little effect on the average normal stress applied by each cell. F) Adjusting springs connecting cells to each other from rigid to compliant reduces the average normal stress applied by each cell. In this figure, the modulus of the cell layer was 1 kPa; for results from simulations with other moduli, see Supplementary Fig. 5.

To test this hypothesis, we developed an FE model consisting of a layer of cells adhered to a substrate having dimensions matching the collagen substrates used in the experiments (Fig. 4A–B). An important component of the model is the forces transmitted between neighboring cells and between cells and the substrate. As in previous studies [35, 36], springs were used to make the cell–cell and cell–substrate connections; the stiffness of the springs was modified to control the magnitudes of cell–cell and cell–substrate adhesions. Rigid springs transmitted the greatest force, and force transmission decreased with decreasing spring stiffness.

We used the model to quantify the effect of substrate curvature on the stress at the cell–substrate interface. For this initial analysis, the spring stiffness was set to be rigid. Our analysis focused on the center of curved region, defined as within 200 μm of the center of the curve. As in a previous study [35], the normal stress fluctuated from negative (compressive) at the center of each cell to positive (tensile) at the edge of each cell. The average stress was significantly affected by curvature, with increasing curvature increasing the average stress (Fig. 4C). This observation is consistent with the experiments that showed greater FTE cell invasion occurring on substrates with greater curvature (Fig. 2B).

The model was then used to assess the impact of altering different mechanical components within the cell layer. First, contractility was reduced by decreasing the contractile strain by a factor of 10. This produced a proportional decrease in the stress at the cell–substrate interface (Fig. 4D). Therefore, if cell–substrate stress is required for cell invasion as hypothesized, the model predicts that reducing cell contractility would reduce invasion. Next, the impact of cell–substrate adhesions was assessed by using compliant springs at the cell–substrate

interface. Interestingly, reducing the cell–substrate connections decreased the fluctuations in the stress but had little impact on the average normal stress applied by each cell (Fig. 4E). According to our hypothesis that cell–substrate stress causes invasion, this finding suggests that changes in cell–substrate adhesion would have no impact on invasion. Lastly, the impact of cell–cell adhesions was quantified by using compliant springs at each cell–cell interface. Reducing the spring stiffness increased the fluctuations in the stress within each cell but reduced the average stress between the cell layer and substrate (Fig. 4F). Importantly, these observations were insensitive to the precise values of spring stiffness used in the simulations. Indeed, a comparison between rigid and intermediate stiffness springs or between intermediate and compliant leads to the same findings, namely that normal stresses depended on curvature, contractility and cell–cell adhesions but not on cell–substrate adhesions (Supplementary Fig. 5). The results were similarly independent of the Young's modulus of the cell layer, which had negligible effect on the results (Supplementary Fig. 5). In sum, the model findings provide a means to test our hypothesis that cell–substrate stresses cause invasion—reducing cell contractility or cell–cell adhesions would reduce cell–substrate stresses, which in turn is hypothesized to reduce cell invasion, while reducing cell–substrate adhesion would have no impact.

Experiments confirm a role for contractility and cell–cell adhesion in invasion

To test predictions of the FE model that invasion depends on contractility and cell–cell adhesions but not on cell–substrate adhesions, cells were seeded on collagen I substrates with high curvature and treated with drugs targeting contractility, cell–substrate adhesion and cell–cell adhesion. Blebbistatin, a selective inhibitor of myosin II [49], was used to reduce overall cell contractility. When cells on curved collagen I hydrogels were treated with blebbistatin, there was a significant decrease in both the number of invading cells (Fig. 5A) and the average distance each cell invaded (Fig. 5B). This is consistent with the predictions of the model showing reduced contractility that reduces the stress at the cell–substrate interface (Fig. 4D) and with the fact that myosin II activity is essential for cell migration and invasion [50].

We next assessed the impact of cell–substrate and cell–cell adhesions on invasion. Cell–substrate adhesions were reduced with FAK Inhibitor 14, which blocks FAK phosphorylation [51]. This intervention had no impact on either the number of invading cells (Fig. 5C) or cell invasion distance (Fig. 5D). Finally, cell–cell adhesions were inhibited by using EGTA to chelate calcium ions, which are necessary for cadherin function [52]. EGTA significantly reduced the number of cells that invaded on curved substrates (Fig. 5E). These findings can be explained by our hypothesis that stresses at the cell–substrate interface affect initiation of invasion: the FE model shows that cell–cell adhesion, but not cell–substrate adhesion, affects the normal stress applied by cells to the substrate. Similarly, the experimental data confirm that reducing cell–cell adhesion, but not cell–substrate adhesion, reduces invasion. Interestingly, the average cell invasion distance was unaltered by EGTA (Fig. 5F), which may suggest that cell–cell forces transmitted through cadherins impact the initiation of invasion but have minimal effect on invasion once a cell has initiated the process.

EGTA chelation of Ca^{2+} ions may have effects outside of cadherins through other calcium-dependent signaling pathways. Therefore, to confirm a role for cell–cell adhesion, we sought to verify these findings through alternative approaches. First, FTE cells were seeded sparsely on conditions with high curvature such that there were essentially no cell–cell adhesions. Consistent with the model predictions and the results from EGTA, the loss of cell–cell adhesions resulted in a complete loss of invasion (Supplementary Fig. 6A). Secondly, we sought to establish a relationship between invasion and the specific cadherin involved. As N- and E-cadherin are the two main adhesion proteins in adherens junctions, confluent monolayers of FTE cells were immunostained for each protein. Fluorescent imaging demonstrated that confluent FTE cells expressed N-cadherin but not E-cadherin at their cell–cell junctions (Fig. 6A and B), indicating that N-cadherin is likely a major cell–cell adhesion protein in FTE monolayers (controls without primary antibodies can be seen in Supplementary Fig. 6B). We therefore specifically blocked N-cadherin using a blocking antibody added to the cells prior to initiation of culture and formation of cell–cell junctions. Addition of this blocking antibody had no impact on initial seeding density (Supplementary Fig. 6C). With this treatment, FTE cells displayed a significant reduction in the number of invad-

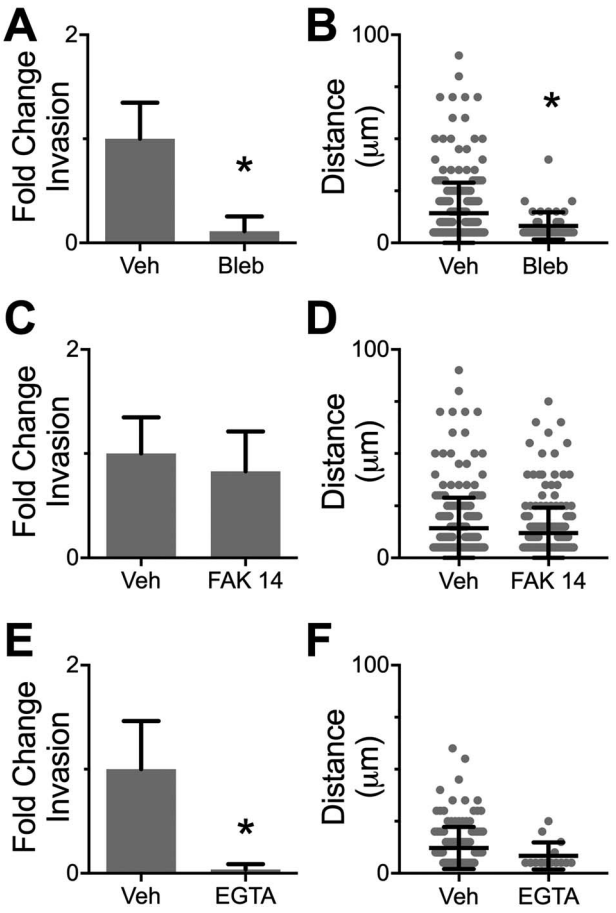

Figure 5. The impact of drug inhibitors on FTE cell invasion on substrates with high curvature. A) Blebbistatin decreased the number of invading cells. $n = 18$ gels for vehicle and 6 gels for blebbistatin. B) Blebbistatin decreased the average distance of invasion. $n = 253$ cells for vehicle and 44 cells for blebbistatin. C) FAK inhibitor 14 did not impact the number of invading cells. $n = 18$ gels for vehicle and 8 gels for FAK inhibitor 14. D) FAK inhibitor 14 did not impact invasion distance. $n = 253$ cells for vehicle and 235 cells for FAK inhibitor 14. E) EGTA decreased the number of invading cells on curved substrates. $n = 19$ gels for vehicle and 14 gels for EGTA. F) EGTA did not impact invasion distance. $n = 149$ cells for vehicle and 15 cells for EGTA. * indicates $P < 0.01$ using a two-sided t-test.

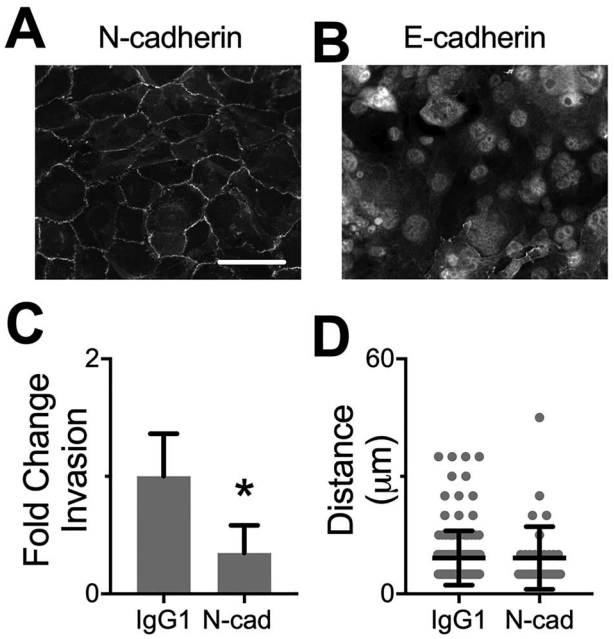

Figure 6. Blocking N-cadherin interactions decreased FTE cell invasion from substrates with high curvature. A) and B) Immunofluorescent staining for N-cadherin and E-cadherin in FTE cells showed the presence of N-cadherin but not E-cadherin at cell–cell junctions. Scale bar = 25 μm. C) Treatment with an N-cadherin blocking antibody decreased the number of invading cells. $n = 8$ gels per condition. * indicates $P < 0.001$ by two-sided t-test. D) Treatment with an N-cadherin blocking antibody did not impact invasion distance. $n = 135$ cells for IgG1 and 35 cells for N-cadherin-blocked condition.

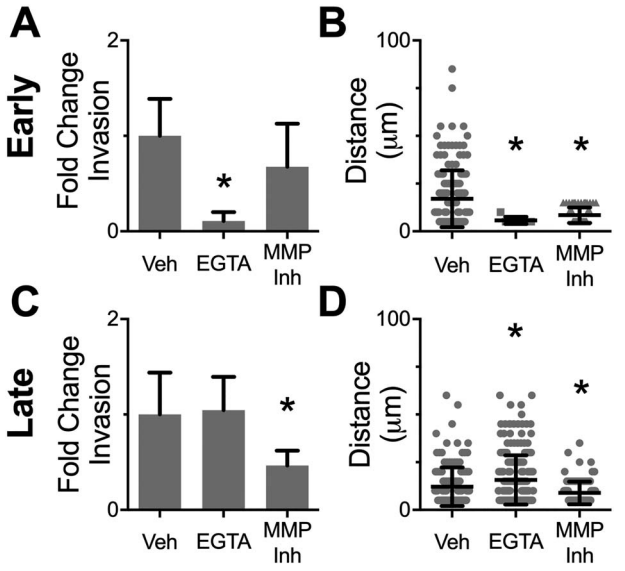

Figure 7. EGTA and MMP inhibitors impacted invasion from substrates with high curvature on different timescales. A,B) To examine the impact of early inhibition, cells were treated 1 h after seeding and invasion was measured at 24 h. A) EGTA decreased the number of invading cells, while MMP inhibitors had no significant effect. $n = 8$ gels per condition. B) Both EGTA and MMP inhibitors decreased the average invasion distance. $n = 170$ cells for vehicle, 7 cells for EGTA and 65 cells for MMP inhibitors. C, D) To examine the impact of inhibition once invasion had begun, cells on curved substrates were treated 24 h after seeding and invasion was measured at 72 h. C) EGTA had no effect on the number of invading cells, while MMP inhibitors decreased the number of invading cells. $n = 17$ gels for vehicle, 10 gels for EGTA and 6 gels for MMP inhibitors. D) EGTA treatment increased average invasion distance, while MMP inhibitors decreased average invasion distance. $n = 149$ cells for vehicle, 217 cells for EGTA, and 94 cells for MMP inhibitors. * indicates $P < 0.05$ relative to vehicle control using Dunnett's test.

ing cells compared to isotype control (Fig. 6C). In accordance with EGTA data (Fig. 5F), blocking N-cadherin did not change the distance FTE cells were able to invade (Fig. 6D). It therefore appears that N-cadherin is responsible for the cell–cell adhesion required for invasion. Together with the results of the FE model, these findings demonstrate that initiation of invasion results from a global force balance in the cell layer, which is transmitted through cell–cell adhesions and to the interface between each cell and the substrate. This global force balance can be altered by changing substrate curvature, contractility or cell–cell adhesions with any of these three impacting initiations of invasion.

Cell–cell adhesion and MMP mechanisms of curvature-based invasion act on different timescales

Given that invasion was impacted by both MMPs and cell–cell adhesion, we hypothesized that these two mechanisms influenced different aspects of FTE cell invasion from curved substrates. Specifically, we hypothesized that cell–cell adhesion was involved in the initial step of an FTE cell breaking away from the cell monolayer and invading into collagen I, while MMPs allowed those FTE cells that had escaped the monolayer to invade further into the matrix. To test this hypothesis, inhibitors of cell–cell adhesion (EGTA) or MMPs (blebbistatin and GM6001) were added to cells on substrates with high curvature for either early (1 h after seeding, invasion after 24 h with inhibitors) or later (24 h after seeding and measuring invasion at 72 h) stages of invasion. We selected 24 h as prior observations had suggested that cell invasion was clearly initiated by this time. EGTA was used to inhibit cadherins rather than the N-cadherin blocking antibody as EGTA could be added in the middle of an experiment while blocking antibodies needed to be incubated with FTE cells before seeding to effectively disrupt cell–cell adhesions. EGTA treatment during initial invasion significantly decreased the number of invading cells while MMP inhibitors did not (Fig. 7A). When the distance of invasion was quantified at 24 h, both EGTA and MMP inhibitors significantly reduced FTE cell invasion distance (Fig. 7B). When inhibitors were added to cells on curved substrates after 24 h, EGTA did not impact the number of invading FTE cells while MMP inhibitors significantly decreased invasion number, suggesting that by 24 h, most cells had already initiated invasion yet still required MMPs to invade into the substrate (Fig. 7C). Adding EGTA after 24 h significantly increased invasion distance, while MMP inhibitors significantly decreased FTE cell invasion distance (Fig. 7D). Taken together, these data indicate that initial invasion (during the first 24 h) depended on the global force balance transmitted by the cell–cell junctions. Consistent with this interpretation, high-curvature substrates had significantly more cells that had broken away from the monolayer at 24 h compared to both low curvature and flat gels (Supplementary Fig. 7). In contrast, MMPs promoted invasion throughout the duration of the experiments and governed the distance that FTE cells were able to invade into the matrix.

CONCLUSION

Curvature is a major component of epithelial tissues throughout the body, yet the impact of substrate curvature on the behavior of

confluent monolayers of epithelial cells has not been rigorously investigated. In ovarian cancer, the microenvironmental niche of ovarian CICs has been hypothesized to induce the cancerous progression of cells trapped within these cysts, and our previous work showed that this niche environment can promote FTE cell invasion [21]. Our results demonstrated that cell invasion was influenced by curvature, with more cells invading on substrates with higher curvature and essentially no invasion on flat substrates. Invasion from curved substrates was dependent on MMPs, but did not involve changes in MMP expression. Rather, an FE model predicted that overall cell contractility and cell–cell adhesion were important for curvature-based invasion, while cell–substrate connections did not impact invasion. Our results confirmed this experimentally, identifying N-cadherin as the responsible junctional protein and supporting that cell–cell adhesion was required for contractile forces in the cell layer to be transmitted to the local cell–substrate interface, thus initiating invasion. After cells began to invade, MMPs regulated the distance of invasion. CICs shrink in size during resolution, and this structural change will result in areas with increased curvature within these cysts; our results suggest that cells can sense this change—even though orders of magnitude larger than the cell body—and transition to an invasive phenotype as a result. The work described here provides a foundation for future studies investigating the impact of curvature on epithelial cells and may have implications for metastasis in epithelial tumors that arise in these structures.

SUPPLEMENTARY DATA

Supplementary data is available at *Integrative Biology Journal* online.

ACKNOWLEDGEMENTS

We would like to thank the University of Wisconsin Translational Research Initiative in Pathology laboratory, in part supported by the UW Department of Pathology and Laboratory Medicine and UWCCC grant no. P30 CA014520, for use of its facilities and services and the University of Wisconsin Optical Imaging Core for use of its facilities and services.

CONFLICT OF INTEREST

There is no conflict to declare.

FUNDING

Funding was provided by the NIH [1DP2CA195766-01 to P.K.K., 1R01CA232517 to P.K.K. and 1R21CA227922 to P.K.K and J.N.] and NSF [CMMI-1660703 to J.N.].

REFERENCES

1. Rusby JE, Brachtel EF, Michaelson JS et al. Breast duct anatomy in the human nipple: Three-dimensional patterns and clinical implications. *Breast Cancer Res Treat* 2007;**106**:171–9.
2. Kleitsch WP. Anatomy of the pancreas; a study with special reference to the duct system. *AMA Arch Surg* 1955;**71**:795–802.
3. Nicholson JK. The microanatomy of the distal tubules, collecting tubules and collecting ducts of the starling kidney. *J Anat* 1982;**134**(Pt 1):11–23.
4. Koff SA. Guidelines to determine the size and shape of intestinal segments used for reconstruction. *J Urol* 1988;**140**(5 Pt 2):1150–1.
5. Discher DE, Janmey P, Wang YL. Tissue cells feel and respond to the stiffness of their substrate. *Science* 2005;**310**:1139–43.
6. Carey SP, Martin KE, Reinhart-King CA. Three-dimensional collagen matrix induces a mechanosensitive invasive epithelial phenotype. *Sci Rep* 2017;**7**:42088.
7. Brown XQ, Ookawa K, Wong JY. Evaluation of polydimethylsiloxane scaffolds with physiologically-relevant elastic moduli: Interplay of substrate mechanics and surface chemistry effects on vascular smooth muscle cell response. *Biomat* 2005;**26**:3123–9.
8. Guo WH, Frey MT, Burnham NA et al. Substrate rigidity regulates the formation and maintenance of tissues. *Biophys J* 2006;**90**:2213–20.
9. Farrelly N, Lee YJ, Oliver J et al. Extracellular matrix regulates apoptosis in mammary epithelium through a control on insulin signaling. *J Cell Biol* 1999;**144**:1337–48.
10. Levina EM, Domnina LV, Rovensky YA et al. Cylindrical substratum induces different patterns of actin microfilament bundles in nontransformed and in ras-transformed epitheliocytes. *Exp Cell Res* 1996;**229**:159–65.
11. Svitkina TM, Rovensky YA, Bershadsky AD et al. Transverse pattern of microfilament bundles induced in epitheliocytes by cylindrical substrata. *J Cell Sci* 1995;**108**(Pt 2):735–45.
12. Bade ND, Kamien RD, Assoian RK et al. Rho activation differentially control the alignment of cells and stress fibers. *Sci Adv* 2017;**3**:e1700150.
13. Yip AK, Huang P, Chiam KH. Cell-cell adhesion and cortical actin bending govern cell elongation on negatively curved substrates. *Biophys J* 2018;**114**:1707–17.
14. Broaders KE, Cerchiari AE, Gartner ZJ. Coupling between apical tension and basal adhesion allow epithelia to collectively sense and respond to substrate topography over long distances. *Integr Biol (Camb)* 2015;**7**:1611–21.
15. Fadare O. *Precancerous Lesions of the Gynecologic tract: Diagnostic and Molecular Genetic Pathology*, Vol. **26**. Cham, New York, Springer International Publishing, 2015 Nov, 318.
16. Auersperg N, Wong AS, Choi KC et al. Ovarian surface epithelium: Biology, endocrinology, and pathology. *Endocr Rev* 2001;**22**:255–88.
17. Berchuck A, Kohler MF, Boente MP et al. Growth regulation and transformation of ovarian epithelium. *Cancer* 1993;**71**(2 Suppl):545–51.
18. Banet N, Kurman RJ. Two types of ovarian cortical inclusion cysts: Proposed origin and possible role in ovarian serous carcinogenesis. *Int J Gynecol Pathol* 2015;**34**:3–8.
19. Karst AM, Drapkin R. Ovarian cancer pathogenesis: A model in evolution. *J Oncol* 2010;**2010**:932371.
20. Sharma A, Gentry-Maharaj A, Burnell M et al. Assessing the malignant potential of ovarian inclusion cysts in postmenopausal women within the UK collaborative trial of ovarian cancer screening (UKCTOCS): A prospective cohort study. *BJOG* 2012;**119**:207–19.
21. Fleszar AJ, Walker A, Porubsky V et al. The extracellular matrix of ovarian cortical inclusion cysts modulates invasion of fallopian tube epithelial cells. *APL Bioeng* 2018;**2**: pii: 031902.

22. Endsley MP, Moyle-Heyrman G, Karthikeyan S et al. Spontaneous transformation of murine oviductal epithelial cells: A model system to investigate the onset of fallopian-derived tumors. *Front Oncol* 2015;**5**:154.
23. Ahmed AA, Etemadmoghadam D, Temple J et al. Driver mutations in TP53 are ubiquitous in high grade serous carcinoma of the ovary. *J Pathol* 2010;**221**:49–56.
24. Lee Y, Miron A, Drapkin R et al. A candidate precursor to serous carcinoma that originates in the distal fallopian tube. *J Pathol* 2007;**211**:26–35.
25. Gross AL, Kurman RJ, Vang R et al. Precursor lesions of high-grade serous ovarian carcinoma: Morphological and molecular characteristics. *J Oncol* 2010;**2010**:126295.
26. Zhang Y, Cao L, Nguyen D et al. TP53 mutations in epithelial ovarian cancer. *Transl Cancer Res* 2016;**5**:650–63.
27. Jimenez-Torres JA, Peery SL, Sung KE et al. LumeNEXT: A practical method to pattern luminal structures in ECM gels. *Adv Healthc Mater* 2016;**5**:198–204.
28. Giacomini MM, Travis MA, Kudo M et al. Epithelial cells utilize cortical actin/myosin to activate latent TGF-β through integrin α(v)β(6)-dependent physical force. *Exp Cell Res* 2012;**318**:716–22.
29. Zang M, Zhang Y, Zhang B et al. CEACAM6 promotes tumor angiogenesis and vasculogenic mimicry in gastric cancer via FAK signaling. *Biochim Biophys Acta* 2015;**1852**:1020–8.
30. Tria S, Jimison LH, Hama A et al. Sensing of EGTA mediated barrier tissue disruption with an organic transistor. *Biosensors (Basel)* 2013;**3**:44–57.
31. Chitaev NA, Troyanovsky SM. Adhesive but not lateral E-cadherin complexes require calcium and catenins for their formation. *J Cell Biol* 1998;**142**:837–46.
32. Shiryaev SA, Remacle AG, Ratnikov BI et al. Targeting host cell furin proprotein convertases as a therapeutic strategy against bacterial toxins and viral pathogens. *J Biol Chem* 2007;**282**:20847–53.
33. Lee J, Weber M, Mejia S et al. A matrix metalloproteinase inhibitor, batimastat, retards the development of osteolytic bone metastases by MDA-MB-231 human breast cancer cells in Balb C nu/nu mice. *Eur J Cancer* 2001;**37**:106–13.
34. Klymenko Y, Kim O, Loughran E et al. Cadherin composition and multicellular aggregate invasion in organotypic models of epithelial ovarian cancer intraperitoneal metastasis. *Oncogene* 2017;**36**:5840–51.
35. Notbohm J, Kim JH, Asthagiri AR et al. Three-dimensional analysis of the effect of epidermal growth factor on cell-cell adhesion in epithelial cell clusters. *Biophys J* 2012;**102**:1323–30.
36. Mertz AF, Che Y, Banerjee S et al. Cadherin-based intercellular adhesions organize epithelial cell-matrix traction forces. *Proc Natl Acad Sci USA* 2013;**110**:842–7.
37. Lekka M, Laidler P, Gil D et al. Elasticity of normal and cancerous human bladder cells studied by scanning force microscopy. *Eur Biophys J* 1999;**28**:312–6.
38. Alcaraz J, Buscemi L, Grabulosa M et al. Microrheology of human lung epithelial cells measured by atomic force microscopy. *Biophys J* 2003;**84**:2071–9.
39. Rabinovich YI, Esayanur MS, Moudgil BM. Capillary forces between two spheres with a fixed volume liquid bridge: Theory and experiment. *Langmuir* 2005;**21**:10992–7.
40. Li QS, Lee GY, Ong CN et al. AFM indentation study of breast cancer cells. *Biochem Biophys Res Commun* 2008;**374**:609–13.
41. Scully RE, Young RH, Clement PB. *Tumors of the Ovary, Maldeveloped Gonads, Fallopian Tube, and Broad Ligament: Atlas of Tumor Pathology: Amer Registry of Pathology*, Northfield, IL, College of American Pathologists. 1999, 527 p.
42. Murdoch WJ. Ovarian surface epithelium during ovulatory and anovulatory ovine estrous cycles. *Anat Rec* 1994;**240**:322–6.
43. Paguirigan AL, Beebe DJ. From the cellular perspective: Exploring differences in the cellular baseline in macroscale and microfluidic cultures. *Integr Biol (Camb)* 2009;**1**:182–95.
44. Ziltener HJ, Maines-Bandiera S, Schrader JW et al. Secretion of bioactive interleukin-1, interleukin-6, and colony-stimulating factors by human ovarian surface epithelium. *Biol Reprod* 1993;**49**:635–41.
45. Chene G, Penault-Llorca F, Le Bouëdec G et al. Ovarian epithelial dysplasia after ovulation induction: Time and dose effects. *Hum Reprod* 2009;**24**:132–8.
46. American Cancer Society. *Cancer Facts and Figures 2016*. Atlanta: American Cancer Society, 2016.
47. Lu P, Takai K, Weaver VM et al. Extracellular matrix degradation and remodeling in development and disease. *Cold Spring Harb Perspect Biol* 2011;**3**: pii: a005058.
48. Freeman SA, Christian S, Austin P et al. Applied stretch initiates directional invasion through the action of Rap1 GTPase as a tension sensor. *J Cell Sci* 2017;**130**:152–63.
49. Kovács M, Tóth J, Hetényi C et al. Mechanism of blebbistatin inhibition of myosin II. *J Biol Chem* 2004;**279**:35557–63.
50. Vicente-Manzanares M, Ma X, Adelstein RS et al. Non-muscle myosin II takes Centre stage in cell adhesion and migration. *Nat Rev Mol Cell Biol* 2009;**10**:778–90.
51. Golubovskaya VM, Nyberg C, Zheng M et al. A small molecule inhibitor, 1,2,4,5-benzenetetraamine tetrahydrochloride, targeting the y397 site of focal adhesion kinase decreases tumor growth. *J Med Chem* 2008;**51**:7405–16.
52. Kim SA, Tai CY, Mok LP et al. Calcium-dependent dynamics of cadherin interactions at cell-cell junctions. *Proc Natl Acad Sci USA* 2011;**108**:9857–62.

Supplementary Material

Substrate curvature induces fallopian tube epithelial cell invasion via cell-cell tension in a model of ovarian cortical inclusion cysts

Andrew J. Fleszar[1], Alyssa Walker[1], Pamela K. Kreeger[1,2,3,4,*], Jacob Notbohm[1,2,5,*]

[1]Department of Biomedical Engineering, University of Wisconsin-Madison, Madison, Wisconsin 53706, USA

[2]University of Wisconsin Carbone Cancer Center, University of Wisconsin School of Medicine and Public Health, Madison, Wisconsin 53705, USA

[3]Department of Obstetrics and Gynecology, University of Wisconsin School of Medicine and Public Health, Madison, Wisconsin 53705, USA

[4]Department of Cell and Regenerative Biology, University of Wisconsin School of Medicine and Public Health, Madison, Wisconsin 53705, USA

[5]Department of Engineering Physics, University of Wisconsin-Madison, Madison, Wisconsin 53706, USA

*Corresponding authors, with equal contribution

Pamela K. Kreeger
1111 Highland Ave, WIMR 4553
Madison, WI 53705
kreeger@wisc.edu

Jacob Notbohm
1500 Engineering Dr, 533 ERB
Madison, WI 53706
jknotbohm@wisc.edu

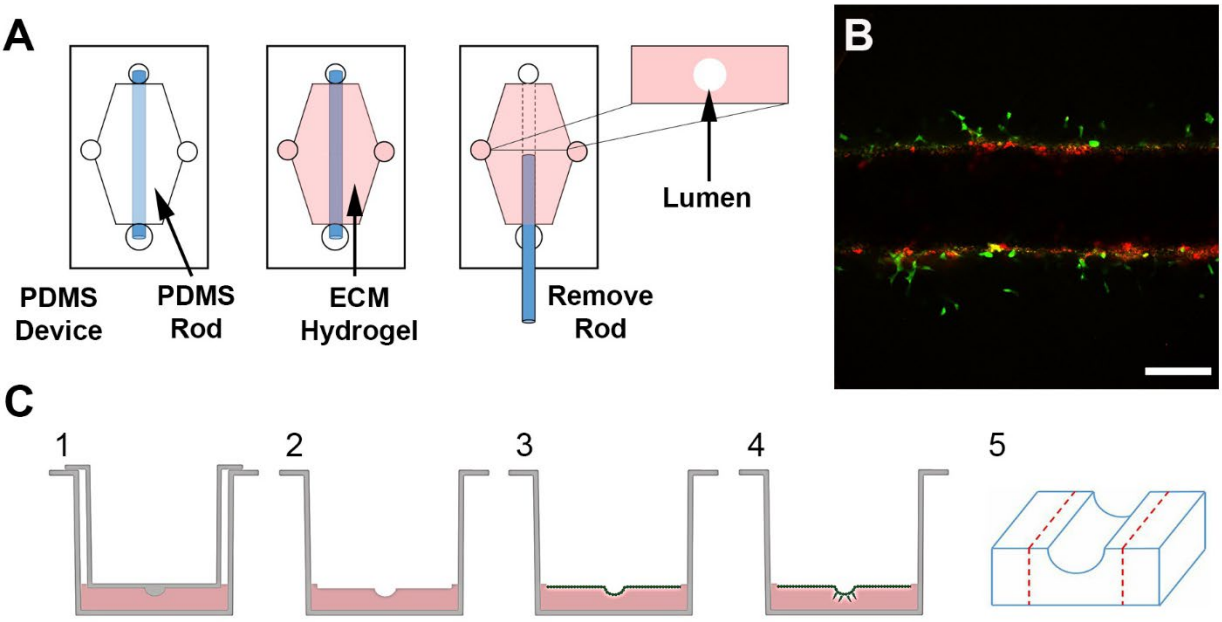

Supplemental Figure 1: A) Schematic of lumen being formed in a microfluidic device. Briefly, an ECM hydrogel (pink) was formed in a PDMS device surrounding a PDMS rod. Upon removal of the PDMS rod, a cylindrical lumen remains within the hydrogel. **B)** Lumen containing a mixture of 50% FTE (green) and 50% OSE (red) cells; cells were labeled with CellTracker dyes prior to initiation of co-culture. In co-cultured conditions, only FTE cells invaded from the lumen into the surrounding ECM. Shown is a representative plane of a z-stack confocal image. Scale bar = 200 µm. **C)** 1) Schematic of a cell culture well containing a mold and collagen gel (pink) formed between the mold and the bottom of the well. 2) Upon removal of the mold, a patterned collagen gel remains. 3) FTE cells (green) are seeded to confluency on the collagen gel. 4) FTE cells invade at the curved region of the gel. 5) Schematic of collagen gel with a curved substrate that was cut into three sections for *Mmp* expression quantification. Red dotted lines indicate cuts, the left and right plateau regions were combined.

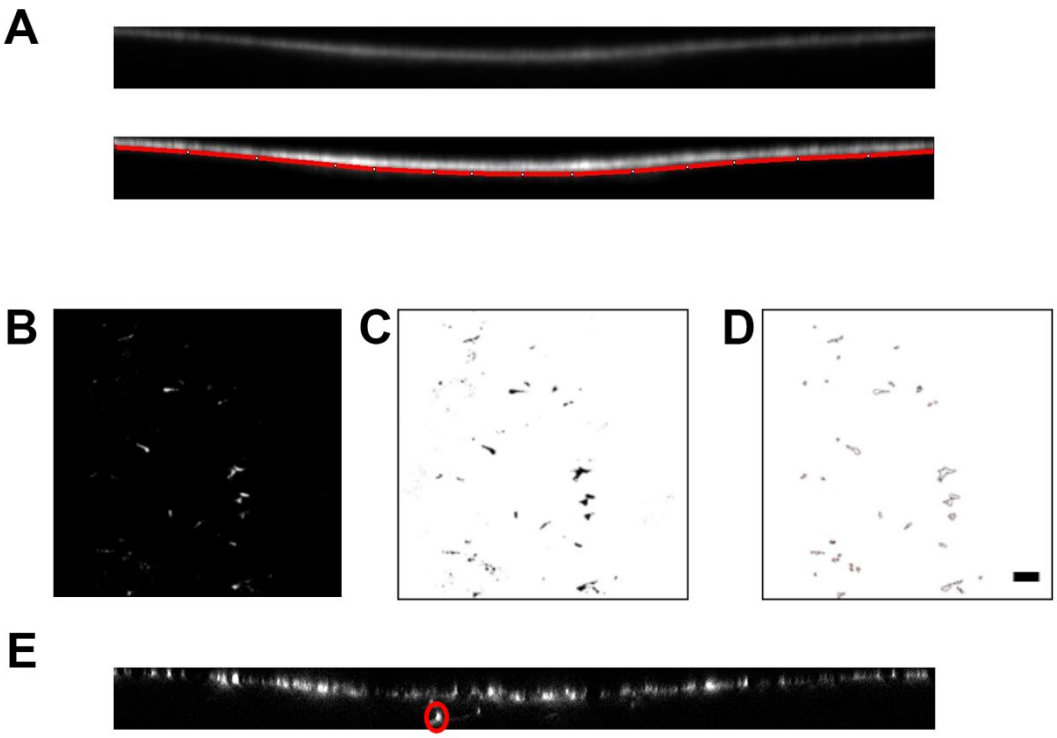

Supplemental Figure 2: Schematic showing the process of analyzing invasion distance and the number of invading cells on curved substrates. **A)** The average intensity of the z-projection side view is used to manually draw the monolayer boundary (red). The area above the red line is deleted from the z-stack. **B)** Top down view of the z-stack after deletion of the monolayer, dots seen are individual cells that invaded. **C,D)** To facilitate automatic counting, cells were thresholded (C) and a cutoff of 40 μm^2 set to identify cell vs. noise (D). Scale bar = 100 μm. **E)** Side view z-section from original stack with an invading cell highlighted (red circle). The distance from the cell to the boundary was manually drawn and measured for each cell.

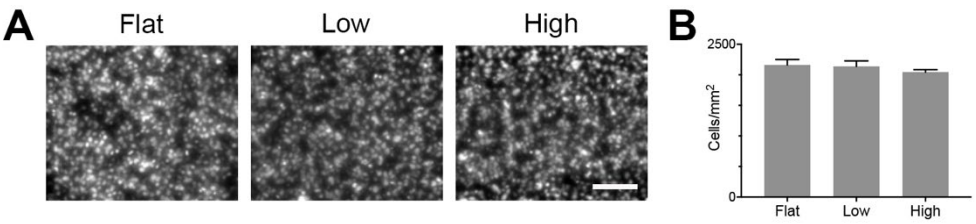

Supplemental Figure 3: A) Representative images of DAPI stained FTE cells after seeding on flat, low curvature, and high curvature collagen gels. Scale bar = 100 μm. **B)** Quantification of nuclei density, accounting for different surface areas due to differences in arc length between conditions. Cell densities were not significantly different, *n* = 4 devices per condition.

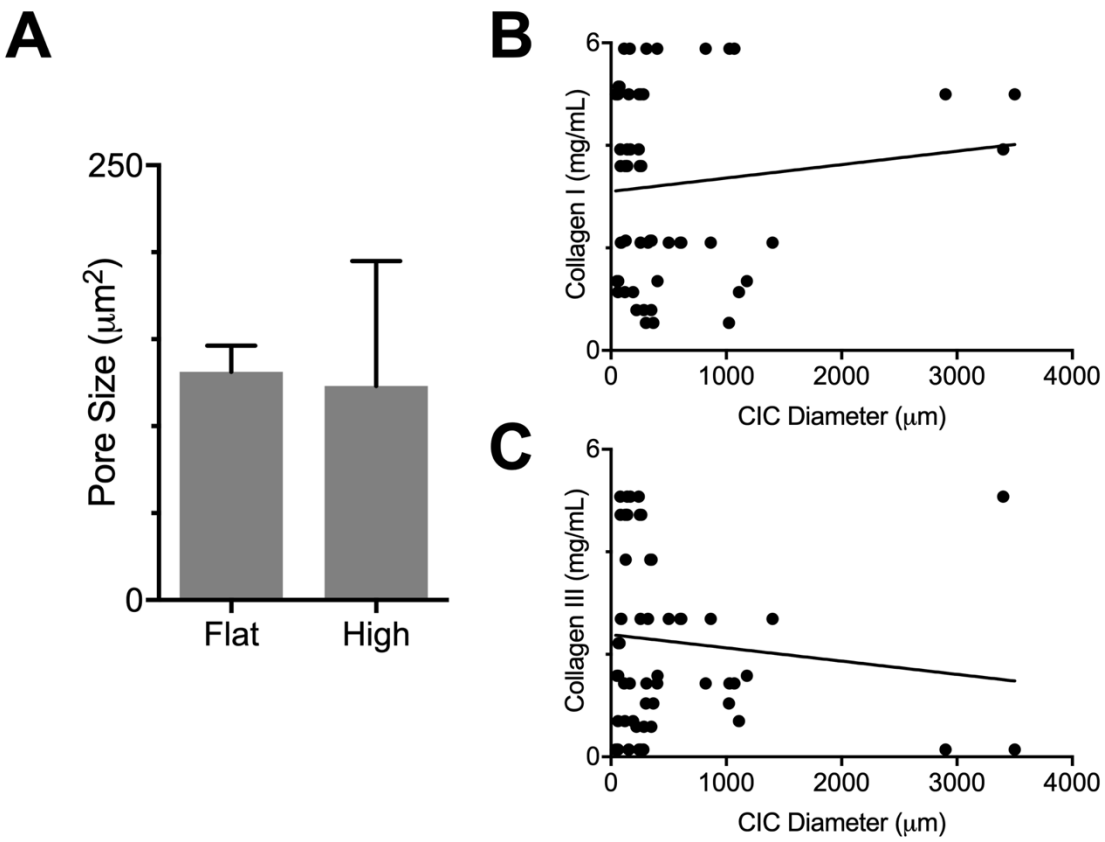

Supplemental Figure 4: A) Collagen gels were stained with CNA35 (1) and the average pore size within gels was measured using Seedwater Segmenter (2). This technique indicates that there is no difference in collagen pore size between flat gels and gels with high curvature. *n* = 3 per condition. **B,C)** The concentration of collagen I (B) and collagen III (C) plotted vs. CIC diameter from archived pathology of human ovaries (original data quantified as aggregate concentrations in (3)). Overall, there was a large amount of variability in collagen concentrations and no strong correlation between ECM concentration and CIC size. $R^2 = 0.01$ for both proteins.

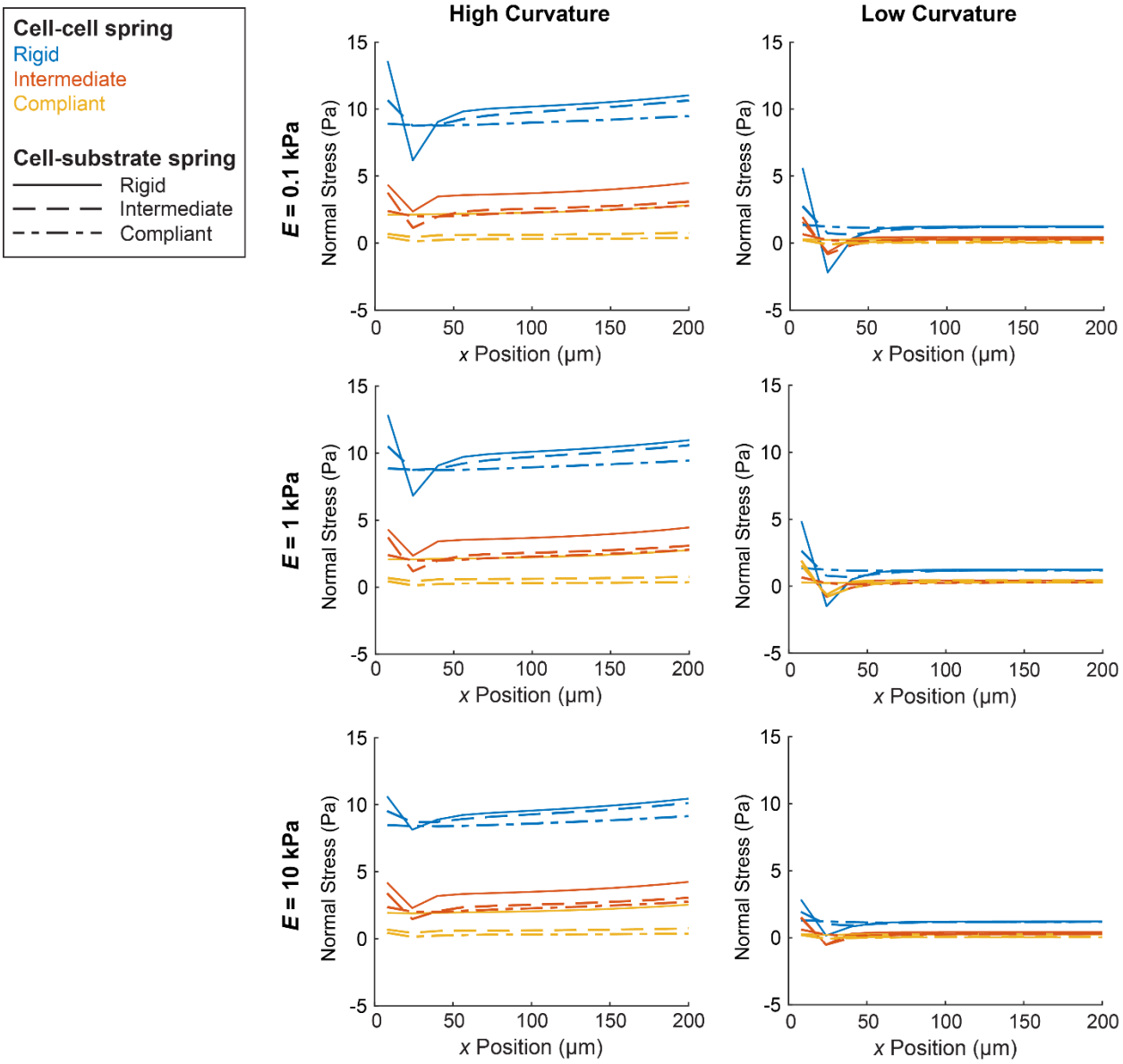

Supplemental Figure 5: Summary of average normal stress between the cell layer and substrate for all combinations of parameters in the model. The Young's modulus of the cell layer was 0.1, 1, or 10 kPa as labeled in the figure. Substrate curvatures were high or low as sketched in Fig. 4B. Cell-cell and cell-substrate spring stiffnesses ranged from rigid to compliant. Contraction of the cell layer was scaled inversely with the modulus; as the model is linear, this scaling affected the magnitudes of stress but not the relative differences due to changing modulus, curvature, or spring stiffness. For all simulations, the Young's modulus of the substrate was 1.7 kPa. In all cases, normal stress was lower on low curvature substrates as compared to high curvature. Additionally, reducing the cell-substrate spring stiffness had little effect on normal stress whereas reducing the cell-cell spring stiffness strongly decreased the normal stress.

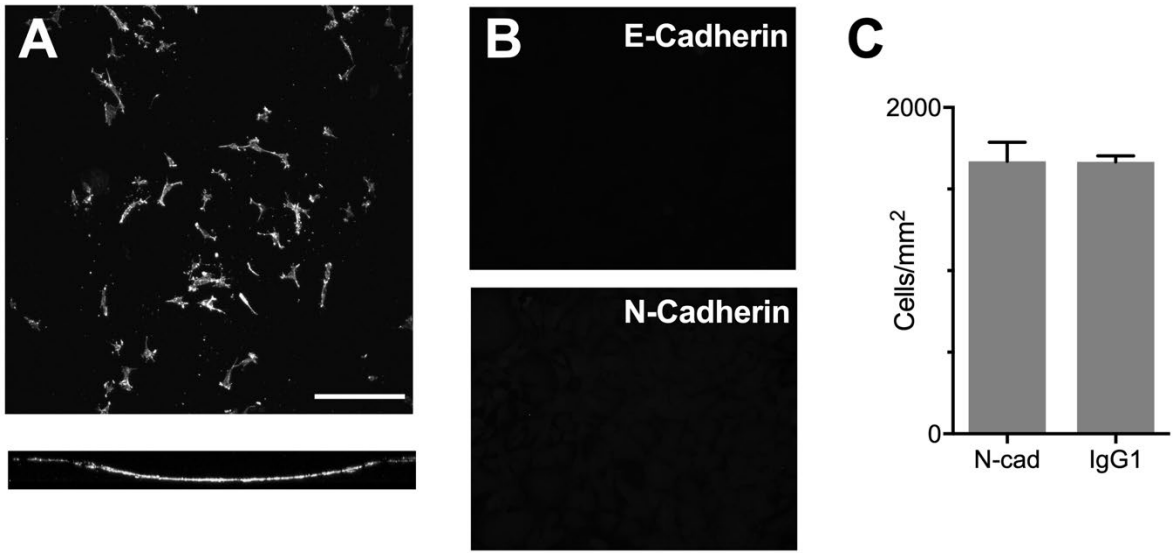

Supplemental Figure 6: A) FTE cells were seeded at 400 µL of 130,000 cells/mL on collagen gels with high curvature. This equates to 10% of the cells seeded in the confluent experiments. A top down z-projection (top) demonstrated that cells do not have cell-cell adhesions. A side z-projection at max intensity (bottom) demonstrated that sparsely seeded cells do not invade on high curvature. Scale bar = 200 µm. **B)** No primary antibody controls for E- and N-cadherin indicate that there was low background fluorescence from the secondary antibodies. **C)** Quantification of cell density on high curvature after treatment with N-cadherin blocking antibody or IgG1 control antibody. Cell densities were not significantly different, $n = 3$ devices per condition.

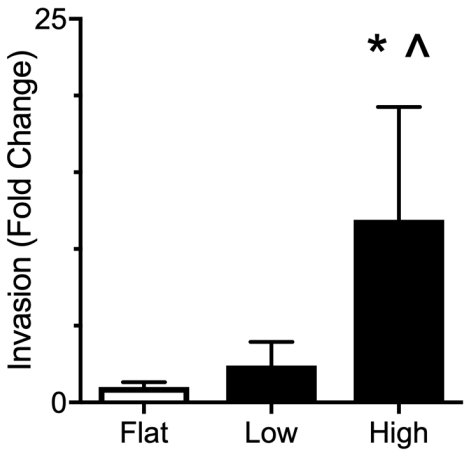

Supplementary Figure 7. The number of invading cells on flat, low, and high curvature collagen gels were measured after 24 hours. High curvature had significantly more invading cells, indicating that cells begin to invade earlier on high curvature. $n = 4$ per condition, * indicates $p < 0.05$ from flat, ^ indicates $p < 0.05$ from low.

References

1. Krahn KN, Bouten CV, van Tuijl S, van Zandvoort MA, Merkx M. Fluorescently labeled collagen binding proteins allow specific visualization of collagen in tissues and live cell culture. Anal Biochem. 2006;350(2):177-85.
2. Mashburn DN, Lynch HE, Ma X, Hutson MS. Enabling user-guided segmentation and tracking of surface-labeled cells in time-lapse image sets of living tissues. Cytometry A. 2012;81(5):409-18.
3. Fleszar AJ, Walker A, Porubsky V, Flanigan W, James D, Campagnola PJ, et al. The Extracellular Matrix of Ovarian Cortical Inclusion Cysts Modulates Invasion of Fallopian Tube Epithelial Cells. APL Bioeng. 2018;2(3).